Marine Geology 411 (2019) 88–97

Contents lists available at ScienceDirect

Marine Geology

journal homepage: www.elsevier.com/locate/margo

Coral reef carbonate record of the Pliocene-Pleistocene climate transition from an atoll in the South China Sea

Wei Jiang[a,b], Kefu Yu[a,b,*], Tianlai Fan[a,b], Shendong Xu[a,b], Rui Wang[a,b], Yu Zhang[a,b], Yuanfu Yue[a,b], Jian-xin Zhao[c], Yue-xing Feng[c], Chaoshuai Wei[a], Shaopeng Wang[a], Yinghui Wang[a,b]

[a] Guangxi Laboratory on the Study of Coral Reefs in the South China Sea, Coral Reef Research Center of China, School of Marine Sciences, Guangxi University, Nanning 530004, PR China
[b] Laboratory for Marine Geology, Qingdao National Laboratory for Marine Science and Technology, Qingdao 266061, PR China
[c] Radiogenic Isotope Facility, School of Earth and Environmental Sciences, The University of Queensland, Brisbane, QLD 4072, Australia

ARTICLE INFO

Editor: Michele Rebesco

Keywords:
Shallow-water carbonate
Sr isotope
Rare earth element
East Asian monsoon
Continental weathering

ABSTRACT

As a natural laboratory for testing various paleoclimatological and paleoceanographic hypotheses, the Pliocene-Pleistocene stratigraphic sequence from a full-coring major scientific drilling (Well CK2 with total length: 928.75 m) in Yongle atoll of Xisha Islands, northern South China Sea was studied. The Petrography of studied section of the core was dominated by reef carbonate limestones which contain abundant shallow marine organisms, e.g., coralline algae, corals, and foraminifera, which almost consisted of pure carbonates and preserved the primary geochemical message since Pliocene. According to the isolation of Well CK2 and the provenance of elements, the systematic changes and abrupt points of isotope and element geochemical compositions (rare earth element parameters, SiO_2 content, Al/Ti ratio, etc.) from coral reef carbonate record presented the elevated terrigenous influences related to the East Asian monsoon after ~2.6 Ma BP, as part of the Pliocene-Pleistocene climate transition. Our results demonstrated that the continental weathering controlled by the East Asian summer monsoon dominated the surface seawater compositions of study area before ~2.6 Ma BP, when the winter monsoon was not strong enough to exert significant influences. Then, the effects of eolian dust associated with the intensity of East Asian winter monsoon, the precipitation driven by summer monsoon, and the global temperature, which played different roles at different periods after ~2.6 Ma BP, should be considered. Our results confirmed that the potentials and significances of shallow-water carbonate deposition from coral reefs, and provided a unique perspective to shed light on the carbonate record of climate changes.

1. Introduction

The global environmental evolution from a warm and uniform climate state into an extreme one with typical glacial-interglacial cycles has greatly enhanced interest in the Pliocene-Pleistocene as a focus in paleoceanography (Du et al., 2016; Herman and Champagnac, 2016; Huang et al., 2005; Jian et al., 2003; Rohling et al., 2014; Shackleton and Opdyke, 1977). In the East Asian monsoon (EAM) region, the Pliocene-Pleistocene is particularly important due to the continued intensification of the East Asian summer and winter monsoons about 3.6–2.6 Ma ago, and the increased variability and possible weakening of the East Asian summer monsoon (EASM), as well as continued strengthening of the East Asian winter monsoon (EAWM) since about 2.6 Ma ago (An et al., 2001). Although it has been widely studied from pelagic and continental records (Huang et al., 2003a; Huang et al., 2005; Jian et al., 2003; Rea et al., 1998; Shackleton, 1995; Sun et al., 1998; Sun et al., 1997; Wan et al., 2012; Wan et al., 2007; Zheng et al., 2000), the lack of in situ, shallow-water carbonate platform sections inhibits interpretations of whether the transition had left geochemical fingerprints in the shallow-water carbonate ecosystems, which are highly sensitive to ocean chemistry and physical processes (Self-Trail et al., 2017; Wilson, 2008). In addition, the reported huge differences of deposition rates between shallow-water and deep-sea sediments in the Pliocene-Pleistocene (Shao et al., 2017b) also complicated the interpretation of paleoclimate records.

Although the geochemical records of shallow-water carbonate have

* Corresponding author at: Guangxi Laboratory on the Study of Coral Reefs in the South China Sea, Coral Reef Research Center of China, School of Marine Sciences, Guangxi University, Nanning 530004, PR China.
E-mail address: kefuyu@scsio.ac.cn (K. Yu).

https://doi.org/10.1016/j.margeo.2019.02.006
Received 27 August 2018; Received in revised form 3 February 2019; Accepted 17 February 2019
Available online 23 February 2019
0025-3227/ © 2019 Elsevier B.V. All rights reserved.

received less attention, recent work on the Xisha carbonate platforms in the South China Sea (SCS) has reconstructed the sea level fluctuations since the early Miocene, and found an abrupt drop in the Pliocene-Pleistocene based on multiple organic/inorganic geochemical proxies of carbonate (Shao et al., 2017a). The SCS is ideally positioned for documenting the palaeoceanographic record to variations of the East Asia monsoon, which in turn is formed by seasonal pressure differences between the western equatorial Pacific and East Asian landmass. More and more interests from paleoceanographers have been attracted to this region. Shao et al. (2017b) reported that the carbonate platform growth in the SCS was the most active in the middle Miocene, decreased in the late Miocene, revitalized in the Pliocene, and active again in the Pleistocene. None but the isolated carbonate platforms on several basement highs survived and continued to develop in the Pliocene-Pleistocene (Hutchison, 2010; Wu et al., 2014).

The isolated carbonate platforms formed far from terrigenous input, whose isolation and thickness made them ideal localities to investigate the record of shallow-water carbonate ecosystem to change in surface ocean temperature and chemistry (Robinson, 2011). These sedimentary systems responded to the changes in the relative abundance of the main carbonate producers and repeated phases of inception, growth, retreat and demise. However, the studies of these invaluable paleoenvironmental archives were often severely hampered by the relatively low stratigraphic resolution of biostratigraphy of carbonate platforms (Frijia et al., 2015) and/or a significant diagenetic overprint of the neritic bulk carbonate chemostratigraphic inventory (Godet et al., 2016). To reveal the potential records of carbonate platform to climate change in the Pliocene-Pleistocene, there is a need for continuous, highly resolved, well preserved and accurate dated shallow-water carbonate records associated with past climate fluctuations.

Abundant geological data on the biostratigraphy, lithology, sedimentology, and paleomagnetism from the scientific and commercial drilling programs conducted in the carbonate platform over the past half century (Shao et al., 2017a; Shao et al., 2017b), however, few early boreholes focused on the coral reef carbonate records of the climate change due to the poor coring recoveries and the rough age structures. Well CK 2, drilled in 2013 on an isolated carbonate platform in the SCS (Fig. 1), with core recovery averages of ~70%, > 80% in most sections, provided very ideal research materials since early Miocene, and thereby permitted an initial assessment of the record of a shallow-water carbonate platform to the climate change. Strontium (Sr) isotope stratigraphy of the platform carbonate was applied, in conjunction with magnetostratigraphy, to refine the stratigraphic framework of the Well. Here we provide an integrated geochemical record of the Pliocene-Pleistocene carbonate platform dominantly composed of limestone from Well CK2 in the northern SCS, with a focus on the records of carbonate platform to the climate changes.

2. Regional setting

The SCS is not only the main area controlled by the EAM, but also the largest low-latitude marginal sea on the globe, originally formed as a result of rapid seafloor spreading during the Cenozoic (Barckhausen and Roeser, 2013). Coral reefs are widely distributed across the SCS, dominated by fringing reefs, platform reefs, and atolls (Yu, 2012), and the developmental history of reefs in the SCS can be dated back to the early Miocene or late Oligocene (Yu and Zhao, 2009). Xisha Islands (17°07′-15°43′N, 111°11′-112°54′E) are a group of atolls situated on an elevated submarine plateau in the northwestern SCS, surrounded by seawater at depths over 1000 m (Fig. 1). Carbonate platforms around the Xisha Islands were widely developed ranging from approximately 310 km^2 to 10,000 km^2 in size (Ma et al., 2011), and the reef and platform growth was relatively active during the middle Miocene, very weak during the late Miocene, and moderate to active during the Pliocene and Pleistocene (Shao et al., 2017b). Xisha Islands are characterized by tropical monsoon climate with annual precipitation from 1300 to 2000 mm, average seawater surface temperature from 22 to 30 °C, and salinity near surface ranges from 33.14 to 34.24‰ (He and Zhang, 1986).

During the past half-century, five wells have been drilled in Xisha Islands, such as Well Xiyong 1 on Yongxing Island in 1970s, Well Xichen 1 and Xichen 2 on Chenhang Island in 1980s, Well Xishi 1 on Shidao Island in 1980s, and Well XK 1 on Shidao Island in 2010s. All the drilling results have provided essential data on biostratigraphy, lithology, development history, and paleoenvironment of the carbonate platform in Xisha Islands. However, few early boreholes focused on the coral reef carbonate records of the climate change due to the poor coring recoveries and the rough age structures. To solve the above issue, Well CK2 was drilled in 2013 on Chenhang Island of the Xisha Islands from an altitude of +1.0 m to a bottom depth of −928.75 m (Fig. 1). The Well CK 2 drilled through the thick Cenozoic carbonate, and can be divided into two sections: carbonate rocks (0–878.21 m) and basaltic volcanic clastic rocks (878.21–928.75 m).

3. Methods

The top ~300 m reef limestone of Well CK 2 in the SCS, were chosen to be densely sampled as research materials according to the category distribution of carbonates and age framework of the whole core in this study. 39 whole-rock powder samples collected at an interval of ~10 m was used to determine mineral species and mass percentages according to 2θ angle and spectral peak intensity by X'Pert PRO diffractometer in the State Key Laboratory of Geological Processes and Mineral Resources, China University of Geosciences, Wuhan. The $^{87}Sr/^{86}Sr$ data was measured with an average of 5 to 10 m intervals at the Radiogenic Isotope Laboratory, University of Queensland. Samples were first washed with 0.25 N acetic acid and then dissolved in 1 N acetic acid prior to column chemistry using Sr-spec resin and was analyzed on a VG Sector-54 thermal ionization mass spectrometer. The Standard SRM987 was routinely analyzed and yielded a mean of 0.710249. The modern seawater standard EN-1 was taken away from a lab by Ken. EN-1's certified value is 0.709175. ~290 samples for carbon and oxygen isotope analyses were obtained from representative hand specimens and were mechanically extracted using a dental drill, followed by powdering in an agate mortar. All the element and isotope samples were analyzed at Guangxi Laboratory on the Study of Coral Reefs in the South China Sea, Guangxi University, China.

An analysis of $\delta^{18}O$ was carried out on a Finnigan MAT-253 stable isotope mass spectrometer that attached to a Fairbanks carbonate preparation device. Powdered samples (approximately 20 mg) were reacted with 100% H_3PO_4 at 75 °C in an automated carbonate device to extract CO_2. Isotopic ratios were reported in the per mil (%) convention and normalized to the Vienna Pee Dee Belemnite (V-PDB) using the GBW04405 standard ($\delta^{13}C = 0.57‰$, $\delta^{18}O = -8.49‰$). Multiple measurements ($n = 15$) of this standard yielded a standard deviation of 0.05% for $\delta^{13}C$, and 0.08% for $\delta^{18}O$. In addition, approximately 20% of all the samples were measured replicates and guarantee the differences between double measurements were within the range of analytical errors. Bulk carbonate samples for elemental analyses were processed and measured with standard techniques using an inductively coupled plasma emission mass spectrometer (ICP-MS). Analyzed data were assessed for accuracy and precision using quality assurance and quality control (QA/QC) program, which included reagent blanks, duplicate test, and certified geochemical reference materials (GBW07129, GBW07133, GBW07135) with deviation < 5%.

The paleomagnetic sampling intervals varied between 5 and 10 m, depending primarily on the lithology, and a set of 52 samples were obtained (Table S1). Samples were taken from the core with a 2.54 cm diameter circular diamond laser-positioning drill in the laboratory. All of the oriented samples were subjected to stepwise Alternating Field (AF) demagnetization using a 2G-755R cryogenic magnetometer. The paleomagnetic measurements were completed based on Tauxe et al.

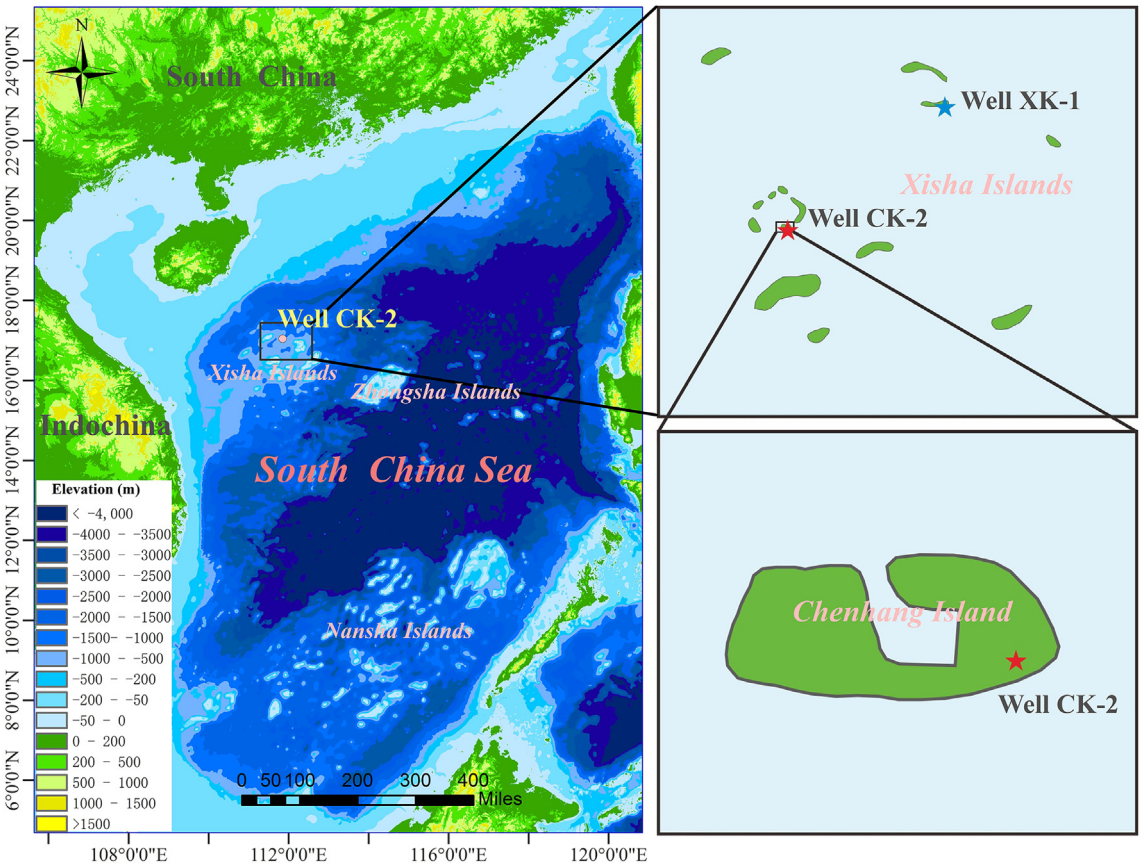

Fig. 1. Locality map of Well CK2 on the Chenhang Island of the Yongxing Atoll and Well XK1 mentioned in the text. The applied bathymetry data were obtained in the Website: https://www.gebco.net/data_and_products/gridded_bathymetry_data/.

(2010) in the paleomagnetism dating laboratory of South China Sea Institute of Oceanology, Chinese Academy of Sciences.

4. Data evaluation and reliability

The primary geochemical message preserved in the marine carbonates, which reflect the seawater chemistry, can potentially be changed by the diagenesis alteration. A series of methods were proposed to evaluate the degree of diagenetic alteration, including Mn/Sr ratios, ^{18}O values, etc. Considering an increase in Mn content and a decrease in Sr content observed during diagenesis, Kaufman and Knoll (1995) proposed that Mn/Sr were important indicators for evaluating the degree of carbonate diagenesis, and the carbonates with Mn/Sr ratios lower than 10 had been suggested to retain a reliable geochemical record. Specially, Derry et al. (1992) and Kaufman et al. (1993) proposed that carbonates that showed Mn/Sr ratios with an upper limit around 2–3 could offer reliable Sr isotopic values. Another principal geochemical signal that was sensitive to diagenesis was the oxygen isotopic composition, which tended to decrease during isotopic exchange with meteoric or hydrothermal fluids. $\delta^{18}O$ values of carbonates higher than −5‰ were observed in the least altered limestone; carbonates with values ranging from −10‰ to −5‰ represented a mild degree of alteration but the effects seemed to be negligible; samples with values below −10‰ were considered unacceptably altered (Derry et al., 1994; Kaufman and Knoll, 1995). In the collected samples, Mn/Sr values ranged between 0.0009 and 0.5040, with an average value of 0.0952. The $\delta^{18}O$ results ranged from −8.79‰ to 4.54‰, with an average of −3.52‰, all of which were above the lower limit of −10‰ (Fig. 2). The correlations between CaO and trace elements have also been used to evaluate the effect of diagenesis, and no correlation between them represented the lack of alteration (Table 1). All these suggested that the trace elements had excellent potential as proxies reflecting variations in seawater chemistry. Well CK2 has been isolated from the mainland since the early Cenozoic, and the collected samples were highly pure coral reef carbonates with high CaO ($CaCO_3$) content over 50% (90%) in most sections (Fig. 3). Therefore, terrestrial materials directly transported by fluvial plumes would not be considered further in this study, and geochemical proxies were mostly related to changes in seawater composition.

5. Results

5.1. Petrography and mineralogy

The Petrography of studied section of the core was dominated by reef carbonate limestones which contain abundant coralline algae, corals, foraminifera, bivalves, and skeletons of other shallow marine organisms, apart from the uppermost section (0–20 m), which was composed of unconsolidated or weakly consolidated sediments. Specifically, the 20–68 m interval contained gray-white coral limestone and calcarenite. The 68–136 m section was mainly composed of light-yellow and flesh pink coral limestone and calcarenite. The section (136–310 m) then became dominated by weakly to moderately cemented bioclastic limestone. X-ray diffraction analysis of the carbonates of Well CK2 (Fig. 3) revealed that the uppermost section (0–20 m), which was mainly composed of aragonite and high-Mg calcite, the mineralogy of the 20–175 m section was composed almost entirely of low-Mg calcite, and the 175–310 m section consisted of low-Mg calcite (~69%) and dolomite (~31%). Considering the reef flat dominating the reef facies above 310 m of the well, the process of diagenetic alteration should be effected by the meteoric diagenesis. To avoid the alteration of diagenesis, the 20–310 m section of Well CK2 was selected as the

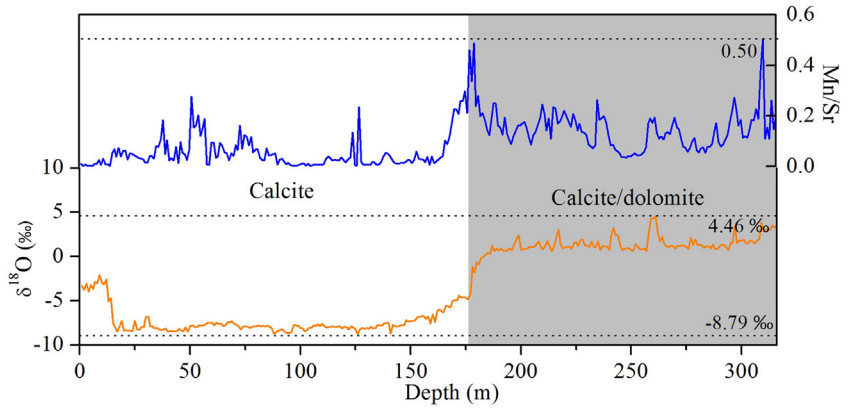

Fig. 2. The Mn/Sr ratio curve and $\delta^{18}O$ curve with depth variations (0–316 m) in Well CK2 (dotted lines and numbers mark data ranges, the white background marks calcite and the gray background marks calcite and dolomite).

research object in this study according to their mineralogical features.

5.2. Stratigraphy and chronology

Strontium-isotope stratigraphy and magnetostratigraphy were applied for cross-dating with independent techniques to improve the accuracy of chronologic framework. In the upper ~300 m section, a total of 43 carbonate samples were collected at interval of 10 m or 5 m around lithological boundaries to conduct Sr isotopic analysis. The $^{87}Sr/^{86}Sr$ ratios of carbonates, especially limestone, have been successfully applied in ancient carbonate records (Aharon et al., 1993; McArthur et al., 2001; McArthur et al., 2016). The $^{87}Sr/^{86}Sr$ ratios range from 0.709037 to 0.709168 (average 0.709102), which belong to those values of the Pliocene-Pleistocene seawater (0.709025–0.709175) (McArthur et al., 2012). Considering that reef carbonates were vulnerable to diagenetic alteration by a variety of pore fluids (e.g., dolomitization) during diagenetic history, bulk rock always contained impurities that affected measured $^{87}Sr/^{86}Sr$ ratios. According to the mineralogy analysis, most samples were composed of low-Mg calcite except several samples (e.g., CK-E316, CK-E321, and CK-E331), which were composed mostly of dolomite. Generally, the $^{87}Sr/^{86}Sr$ ratios of contaminated carbonates by pore fluids presented relatively higher values than original seawater $^{87}Sr/^{86}Sr$ ratios, and they would offer younger ages than the actual ages of carbonates. A total of 19 relatively reliable $^{87}Sr/^{86}Sr$ ratios were selected and converted to numerical ages according to the standard calibrated $^{87}Sr/^{86}Sr$ curve of McArthur et al. (2001), following three criteria as below: 1) $^{87}Sr/^{86}Sr$ ratios monotonically increased upward with the decreasing of depth corresponding to the general increasing trend of Sr isotope evolution of Cenozoic; 2) Abnormal $^{87}Sr/^{86}Sr$ ratios out of stratigraphic order were rejected; 3) Lower $^{87}Sr/^{86}Sr$ ratios were selected for those samples that potentially suffered diagenetic alternation. The $^{87}Sr/^{86}Sr$ ranged from 0.709037 to 0.709168 (Table 2) corresponded to from 5.0 Ma to 0.212 Ma covering the Pliocene-Pleistocene (Fig. 4). It was noteworthy that the rest 24 $^{87}Sr/^{86}Sr$ ratios could also offer important information on the environmental and climate changes.

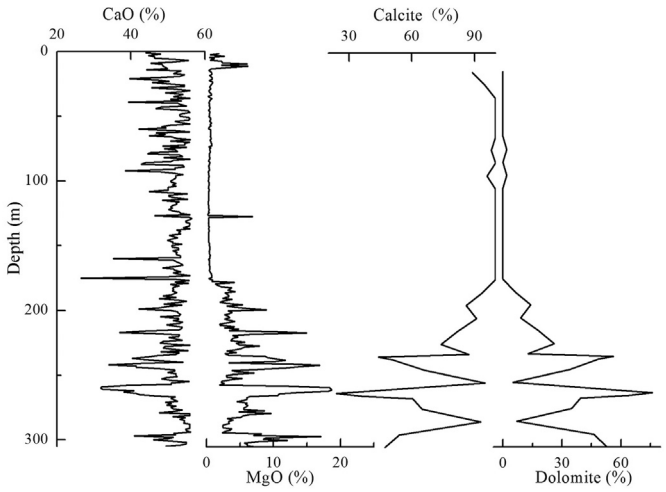

Fig. 3. The contents of carbonate, including CaO and MgO (Left) and the distributions of main minerals, including calcite and dolomite (Right) with depth variations (0–316 m) in Well CK2.

Magnetostratigraphy have been applied successfully in reef sequences in Great Barrier Reef (Braithwaite et al., 2004), Tahiti (Lund et al., 2010; Ménabréaz et al., 2010), Mururoa atoll (Aïssaoui et al., 1990), and New Caledonian (Cabioch et al., 2008) based on reconstruction of polarity chrons succession. Paleoinclinations were

Table 1
The correlations of main elements with depth variations (0–316 m) in Well CK2. Only the significant correlation coefficients ($r > 0.3, p < 0.01$(**)) were presented.

	MgO	CaO	P_2O_5	Zn	SiO_2	Ba	REE	Ti	Al	Zr	Mn	Sr
MgO	1											
CaO	−0.673**	1										
P_2O_5	0.372**		1									
Zn				1								
SiO_2					1							
Ba						1						
REE			0.546**				1					
Ti					0.354**		0.518**	1				
Al			0.493**				0.638**	0.673**	1			
Zr			0.463**				0.658**	0.696**	0.820**	1		
Mn			0.324**				0.321**				1	
Sr	−0.516**		−0.499**				−0.548**		−0.423**			1

Table 2
The Sr isotope data of selected samples of Well CK2 for dating and obtained number ages.

Sample NO.	Depth down core (m)	$^{87}Sr/^{86}Sr$	2s	Minimum age	Mean age	Maximum age
CK2-E21	21	0.709168	0.000011	0.162	0.212	0.268
CK2-E31	31	0.709166	0.00001	0.228	0.282	0.342
CK2-E51	51	0.709162	0.00001	0.366	0.427	0.52
CK2-E61	61	0.709149	0.00001	0.655	0.738	0.823
CK2-E81	81	0.709127	0.000012	1.139	1.181	1.228
CK2-E91	91	0.709115	0.000012	1.276	1.324	1.368
CK2-E101	101	0.709109	0.000013	1.35	1.396	1.448
CK2-E121	121	0.709107	0.000012	1.375	1.423	1.483
CK2-E126	126	0.709103	0.000012	1.425	1.485	1.565
CK2-E136	136	0.709096	0.000009	1.552	1.657	1.768
CK2-E141	141	0.709092	0.000011	1.671	1.776	1.886
CK2-E152	152	0.70909	0.000012	1.727	1.837	1.964
CK2-E201	201	0.709079	0.000012	2.1	2.21	2.32
CK2-E221	221	0.709074	0.000012	2.26	2.37	2.51
CK2-E251	251	0.709067	0.000011	2.52	2.73	3.38
CK2-E271	271	0.709063	0.000011	2.68	3.38	3.68
CK2-E316	316	0.709049	0.000009	4.15	4.45	4.68
CK2-E321	321	0.709048	0.000014	4.23	4.52	4.73
CK2-E331	331	0.709037	0.000012	4.89	5	5.09

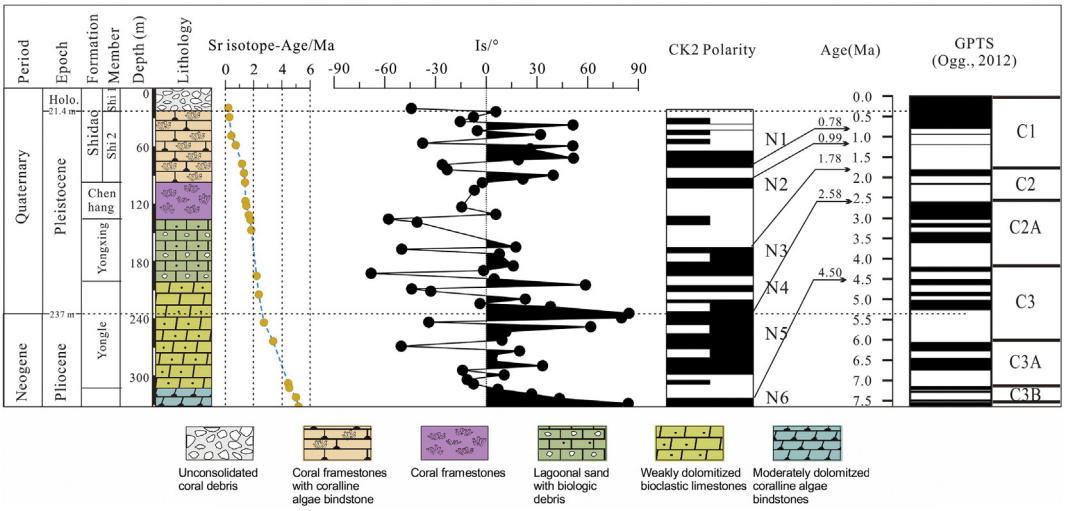

Fig. 4. The age frame of the study, as well as the results of lithostratigraphy, Sr isotope and magnetostratigraphy and their correlation with the GPTS (Ogg, 2012) in Well CK2 (0–316 m).

evaluated and calculated from the vertical projection in orthogonal diagrams. Most of the samples exhibited a well-defined single component magnetization which decayed toward the origin between 30 and 80 mT, suggesting a primary magnetization. For the samples, up inclination corresponded to reversed polarity, whereas down inclination corresponded to normal polarity. Polarity intervals were defined by grouping adjacent sample polarities and matching them to the polarity Chrons and Subchrons of the Geomagnetic Polarity Time Scale (Ogg, 2012). At least two to three successive ChRM directions were required to define polarity zones considering the weak ChRM of carbonates. Ten normal polarities (N1-N10) and eight reversal polarities (R1-R8) were identified (Fig. 4). Based on the Sr age controls, the boundary of the Pleistocene-Pliocene is located at ~237 m in the Well CK2 core.

As shown in Fig. 4, at the top of the CK2, local magnetozone N1 (at a depth range of 0–74 m) should correlate to the chrons C1n to C1r.1n of the GPTS considering that the Sr-ages at 57 m and 74 m were 0.61 Ma and 1.026 Ma, respectively. The magnetozone R2 between 107 and 166 m was characterized by a distinctive reversal with a potential normal polarity, and this pattern appeared to be correlated with chrons C1r to C2n of the GPTS. The magnetozones N3-N5 between 166 and 295 m were dominated by three normal and two reversal polarities, and some potential short events occured in N5 and N6. Finally, the magnetostratigraphic record was established and correlated with GPTS using Sr-age control points. On the basis of these correlation and Sr ages, we suggested that the present polarity chronozones extends from Chron C6 at ~316 m to present at the top.

5.3. Elemental and isotope geochemistry

As the most characteristic elements, CaO ranged from 26.48 to 56.43%. MgO came second in abundance with 0.19–21.59%, showing a mirroring pattern with the abundance of CaO (Fig. 3). Interestingly, most proxies were characterized by a common inflection point at a depth of the Pleistocene/Pliocene boundary. As a terrestrial type element, the SiO_2 was rare, below 0.27%, marked by numerous high-value anomalies in samples from the late Pliocene to early Pleistocene (Fig. 5). As nutrient elements both supplied mainly by terrestrial input, marine transgression or upwelling (Kinsey and Davies, 1979; Saltzman, 2005), P_2O_5, ranging from 0.04 to 0.32%, and Ba, ranging from 1 to 184 ppm, showed a similar trend with peaks in the Pliocene-Pleistocene climate transition (Fig. S1). Unlike other elements, Zn contents suffered an abrupt shift from stable and low values to sharply fluctuant and high values at ~2.21 Ma (Fig. S1). Similar to Zn, the rare earth element (REE) contents also changed from relatively stable and low values to

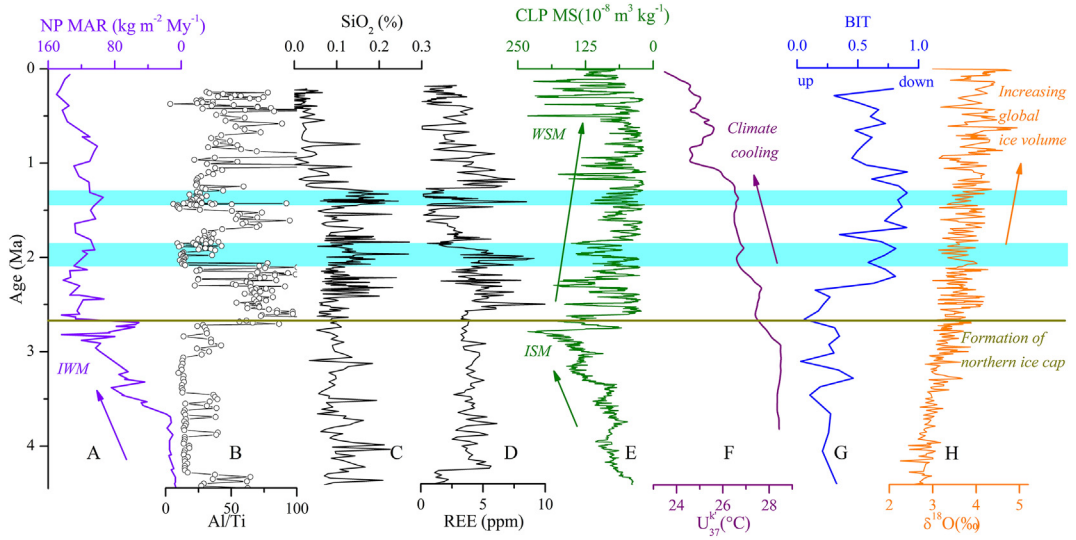

Fig. 5. A comparison of North Pacific (NP), SCS, Chinese Loess Plateau (CLP), and global paleoenvironmental records since ~4.45 Ma BP. (A) NP dust mass accumulation rate (MAR) (Rea et al., 1998). (B) Al/Ti ratios of Well CK2 in the northern SCS. (C) SiO_2 contents of Well CK2 in the northern SCS. (D) REE contents of Well CK2 in the northern SCS. (E) Magnetic susceptibility record on the CLP (Guo et al., 2002; Song et al., 2001). (F) $U_{37}^{K'}$-SST record (0.2 Ma running mean) from ODP Site 1147/1148 in the northern SCS (Jia et al., 2008) (G) BIT data (proxies of local sea level variations) of Well XK1 in the northern SCS (Shao et al., 2017a). (H) Benthic oxygen isotope record in the northern SCS (Wang et al., 2003). The cyan shaded areas were discussed in the text. IWM: intensified winter monsoon; ISM: intensified summer monsoon; WSM: weakened summer monsoon. (For interpretation of the references to colour in this figure legend, the reader is referred to the web version of this article.)

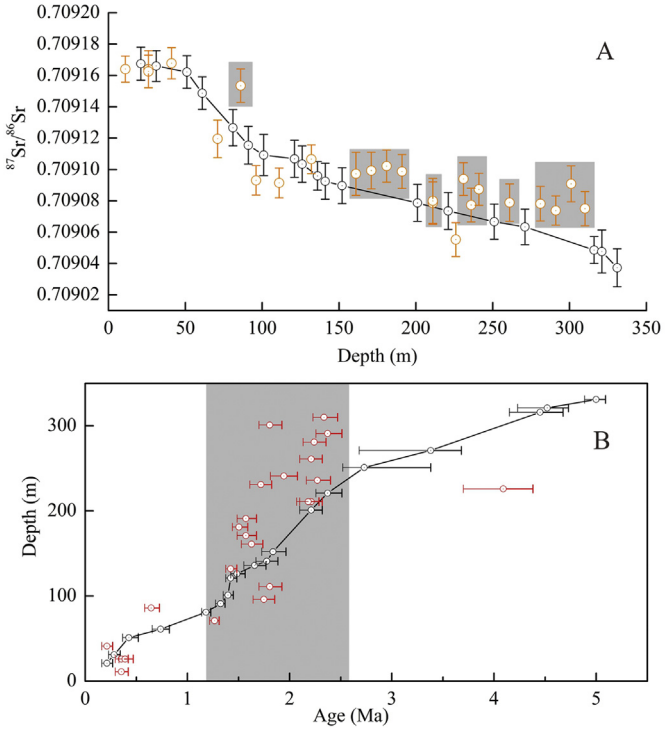

Fig. 6. The diagram of results of Sr isotopes (A) and the distributions of age based on Sr isotopes (B) with depth variations (0–316 m) in Well CK2. The black data were used for dating, and the orange and red ones were other original data. The gray shaded areas were stressed in the text. (For interpretation of the references to colour in this figure legend, the reader is referred to the web version of this article.)

intense oscillations (Fig. 5). Different from Zn, the abrupt shift timeline of REE is ~2.62 Ma. Comparaed to REE contents, the other REE parameters, such as Ce/Ce*, Eu/Eu*, and Nd_N/Yb_N, changed at smaller ranges (Fig. S1). Detrital elements, such as Al, Zr and Ti, preferentially accumulated in clay sediments and generally rose superior to biogenic or diagenetic processes (Cantalejo and Pickering, 2014). It has been suggested that Al, Zr and Ti were ideal proxies for tracing terrigenous materials in marine sediments. Moreover, the strong correlations among Al, Zr and Ti demonstrated that all were mainly of lithogenic origin. Detrital component ratios, such as Al/Ti and Zr/Ti, remained stable before ~2.62 Ma, indicating the relatively stable and single source of detrital matters, but then fiercely fluctuated (Fig. 5 and S1). Most $^{87}Sr/^{86}Sr$ ratios which were excluded from the age frame exhibited higher values, and mainly distributed during ~2 Ma to ~2.62 Ma, indicating extra source of Sr (Fig. 6). The results of major and minor elements, as well as their ratios, were presented in the Fig. S1, and only the most relevant elemental and isotopic data were summarized in Figs. 5 and 6.

6. Discussion

6.1. Interpretation of coral reef carbonate geochemical record

Major or trace elements present in seawater are either dissolved or absorbed onto particles, which are further removed and deposited into sediments through biotic or abiotic processes. Shao et al. (2017a) has confirmed that the element proxies from bulk carbonates were reliable tools for reconstructing the evolution of carbonate platforms. Here, we presented Sr isotope analyses, as well as major and trace element compositions, of bulk carbonate samples from the Well CK2 in the northern SCS. In geochemical analysis, specific elemental ratios could be used as geochemical fingerprints to constrain sediment provenance. Although rather low elements, e.g., Al, Ti and Zr, of carbonates, indicated a far offshore setting with limited terrestrial influence, their signals could still provide unique information on terrestrial inputs. Notably, detrital component ratios, such as Al/Ti and Zr/Ti, remained stable throughout the carbonate sequence during Pliocene, but suffered an abrupt change at ~2.6 Ma BP, indicating the complication of terrestrial input pathways (Fig. 5 and S1). By coincidence, some elements, e.g., REE and SiO_2, also exhibited distinct fluctuation characteristics before and after ~2.6 Ma BP (Fig. 5).

Based on a large number of works, which reported REE patterns of

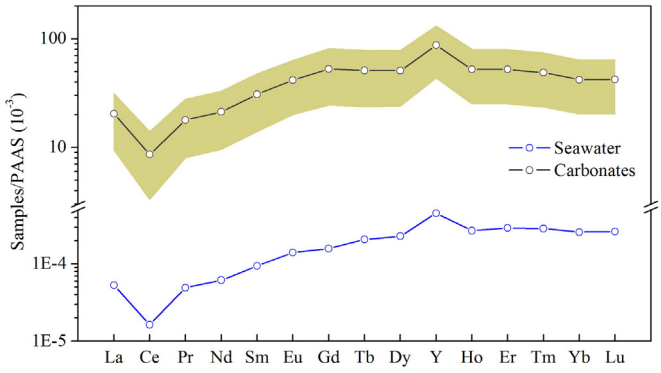

Fig. 7. The PAAS- normalized REE patterns (Taylor and McLennan, 1985) of surface seawater samples from SCS and carbonates in the Well CK2 (0–316 m). The REE curve and the brown shaded area represented the average ± standard deviation area. The data of SCS seawaters is from Alibo and Nozaki (2000). (For interpretation of the references to colour in this figure legend, the reader is referred to the web version of this article.)

carbonates deposited throughout the Phanerozoic that closely resembled the ones of modern seawater (de Paula-Santos et al., 2018; Siahi et al., 2018), the REE chemistry of nearly pure carbonate could present the contemporaneous seawater (Webb and Kamber, 2000), and be applied to track secular marine paleoenvironmental variations. REE enrichment levels and distribution patterns could provide substantial information about the sources of REEs. The seawater signature of the shale normalized REE values in carbonates included the depletion in light REE compared to the heavy REE, a positive La anomaly, a negative Ce anomaly, a small positive Gd anomaly, and superchondritic Y/Ho ratios, as shown in Fig. 7. Specially, Y and Ho exhibited similar ionic radii and chemical behavior, but Ho was scavenged by particulates or ionic species at about twice the rate of Y from the water column of the modern ocean. This process generated a Y/Ho ratio of ~60–70 for seawater compared to ~25–30 for terrigenous materials (Mclennan, 2013). In bulk carbonates, higher Y/Ho represented a larger fraction of seawater-derived REE, and lower Y/Ho thus represented a larger fraction of terrigenous-derived REEs. The average Y/Ho ratio of study samples was ~47, reflecting the combined effects of seawater and terrigenous materials (Fig. S1). Generally, REE could be delivered to seawater from continents via atmospheric dust, terrestrial runoff and marginal sediments (Hathorne et al., 2015). Adjacent to the Neogene Hainan mantle plume, volcanic material should be another possible important contributor of Xisha Islands. However, the PAAS-normalized REE patterns without distinct interruptions ruled out this possibility, due to the discovery by Wu et al. (2018) that the surface seawater REE pattern effected by the volcanic eruptions showed a significant discrepancy from the baseline signatures. Considering the extremely limited influence time of volcanic eruption compared to the relatively low temporal resolution (~10–20 ka) of our study, we believed that the effects on Xisha Islands from the volcanic eruptions should be beyond doubt, but the related imprints could not be recognized in the present study. Therefore, the volcanic materials were left out of consideration in this study. The dominate sources of dissolved REE in the SCS were fluvial and coastal input to the surface ocean, while the Asian dusts, which contained abundant REE, can also altered the surface seawater REE compositions (Jiang et al., 2018). Similar to REE, Si was also considered as a terrestrial type element for its wide distribution in a much wider range of minerals, e.g., glauconite, clay minerals and detrital quartz from eolian sources (Jarvis, 2001). In fact, most representative elements of terrigenous materials, including REE and Si, covaried with each other (Fig. 5), which reflected the elevated terrigenous influences after the Pliocene, coinciding with the systematic changes in sediment fluxes and strontium isotope changes (Figs. 6 and 8).

The dramatic increases of some elements since the Pliocene were also observed in the Well XK1 in Shidao Island of Xisha Islands, when the water depth was shallow according to the reconstructed sea level changes (Shao et al., 2017a), and it maybe reflect the rapid input of continent-derived sediments due to the intensive activity of the EAM. As a whole, most areas in the northern SCS, even where is farther from the mainland, should be inevitably affected by terrigenous sediments from the surrounding landmasses over a long time scale due to its marginal setting. In addition, the significance of dust deposition into the sea on climate change either by direct or indirect interactions with oceanic biogeochemistry or atmosphere during the Quaternary has been synthetically studied (Xu et al., 2015). At suborbital and millennial time scales, nutrient elements, e.g., iron, Al and Si, as well as REE contents in marine sediments have been confirmed to provide direct quantitative estimates of eolian dust deposition in the tropical western Pacific (Kondo et al., 2007; Wang et al., 1999a, 1999b; Xu et al., 2015; Xu et al., 2014), and contribute to elevated primary productivity (Lamy et al., 2014; Martínezgarcía et al., 2014; Murray et al., 2012; Shao et al., 2011; Xiong et al., 2013), supported by the significant correlation between Asian dust input and paleoproductivity (Li et al., 2011b; Xu et al., 2015; Zhang et al., 2007), as well as modern observation (Li et al., 2004). Thus, the above element geochemical records of carbonates should be closely associated with the terrigenous materials transported by dynamic currents or winds, which have also been confirmed to contribute to the enrichment of land-based biomarkers and then the relative high BIT values in the Well XK1 during Pleistocene (Shao et al., 2017a). Furthermore, considering the relative isolation of the carbonate platform far from continent, the winter monsoon should play a crucial role in the migration of terrigenous materials.

6.2. *Coral reef carbonate record of the Pliocene-Pleistocene climate transition*

Major global trends in the Cenozoic include the transition from greenhouse to icehouse conditions (Zachos et al., 2001), radical variations in atmospheric CO_2 levels (Pagani et al., 2005), and the development of the monsoons (An et al., 2001). Additionally, plate tectonic reorganization, eustasy, oceanography and trophic resources are all involved in environmental feedback loops, strongly influencing marine systems (Halfar and Mutti, 2005; Wilson, 2008). The Asian monsoon has long been argued to be a product of the Himalaya-Tibetan Plateau for its key role in transforming regional atmospheric and oceanic circulations (Molnar et al., 2010). Previous studies have suggested that the EAM controls the surface currents and the distribution of nutrients (Cheng et al., 2005; Huang et al., 2003b; Wang et al., 1999a). After ~2.6 Ma BP, the EASM, reflected by the magnetic susceptibility index, became more variable and at times weaker (Fig. 5), but the EAWM, reflected in the indices of the grain-size fraction and Al flux, continued strong, and even intensifies, as does the eolian flux to the North Pacific (An et al., 2001; Clemens et al., 1996; Rea et al., 1998). In the northern SCS, the verified proxies of the EAWM strengthening, e.g., *Neogloboquadrina dutertrei* abundance and planktonic $\delta^{13}C$ (Jian et al., 2003), changed significantly for the 3.2–2.2 Ma period, illustrating the trend of gradual increase in the EAWM, consistent with the conspicuous strengthening of loess accumulation in China and the formation of the Northern Hemisphere ice sheet (An et al., 2001; Liu et al., 1999; Shackleton et al., 1984). These proxies record also implied that the EAWM rapidly increased at ~2.7–2.5 Ma, and there were several fluctuations in the winter monsoon intensity after ~2.2 Ma BP (Jian et al., 2003). Strong fluctuations in most proxies (e.g., REE and SiO_2) since the early Pleistocene seemed to echo the enhanced terrestrial components linked with the intensified winter monsoon following the expansion of the Northern Hemisphere ice sheets about 2.5–2.7 Ma ago (Li et al., 2011a) at glacial sea-level lows (Wei et al., 2006; Wei et al., 2003).

Nevertheless, the overall trends of REE and SiO_2 after ~1.3 Ma tended to weaken (Fig. 5). Considering the provenance of continental

substances and the variation trends of East Asian summer and winter monsoons, it might be contributed by the reduced continental weathering related to the decreased precipitation driven by weakened summer monsoon intensification and climate cooling. One side, the reduced continental weathering could decrease the fluvial and coastal input of terrigenous materials; on the other side, it could also impact the release of sediments from parent rocks for wind to pick up. Recent studies have confirmed that precipitation decrease can potentially decrease erosion (Nie et al., 2018; Nie et al., 2015), resulting in less dust transport to the Pacific Ocean in the late Cenozoic. Thus, the dust accumulation decrease could be achieved via erosion decrease driven by monsoon precipitation when there were sediments available to be transported by the wind (Nie et al., 2018), as opposed to only reduced continental aridity. The local eustatic change was another non-negligible factor, which contributed to controlling factors of reef carbonate buildup. The relative sea level in northern SCS was declining throughout the Pleistocene, in spite of a few deviations from the general trend (Shao et al., 2017a). In this study, we compared the elemental proxies to the reported sea-level curve by Shao et al. (2017a) in the northern SCS. Though the desynchronies in time series between them existed, the possible influences of sea level changes on the elemental proxies of coral reef carbonates could not be ignored for the discrepancies and accuracies of two age frames. After ~1.3 Ma, the sea level turned relatively higher than the previous stage of ~1.3 Ma-~2.3 Ma (Fig. 5), leading to the drowning of a large shelf area during sea level high-stands, might contribute to the overall declines of carbonate REE and Si contents. Although associations between certain elemental excursions and sea-level changes have been examined by Shao et al. (2017a), the behaviors and distribution patterns of those elements still remained subject to multiple controls.

Though the detrital component ratios, e.g., Al/Ti, suffered an abrupt change at ~2.6 Ma BP compared to the relative stable sequence during Pliocene, two intervals at ~2 Ma and 1.3–1.5 Ma BP exhibited similar levels to the Pliocene, revealing that the coincident similar provenance of terrigenous materials. According to the Fig. 5 and above analysis, we considered that the abrupt change at ~2.6 Ma BP of most proxies of our carbonates should be attributed to the intensified winter monsoon. We believed that the impact range or intensity of EAWM reached a threshold for Xisha Islands in the northern SCS at ~2.6 Ma BP, and then lead to the variations of terrigenous constituents through the transportation of eolian dust. Specially, at ~2 Ma and 1.3–1.5 Ma BP, the reduced winter monsoon supported by the North Pacific dust as shown in Fig. 5, as well as the relative abundance of *Neogloboquadrina dutertrei* and the planktonic $\delta^{13}C$ by Jian et al. (2003), should be responsible for the similar levels of detrital component ratios. In fact, REE and SiO_2 contents also showed fluctuant values at these intervals, in accordance with the fluctuations of the EAM. In addition, the monsoon precipitation and temperature, represented by the Chinese Loess Plateau magnetic susceptibility and $\delta^{18}O$ of ODP 1148 as shown in Fig. 5, also played significant roles. At ~2 Ma BP, the REE and SiO_2 contents of carbonates both started to increase and reached the high peaks (Fig. 5). The relatively stronger EASM and the relatively weaker EAWM may be responsible for the high peaks. The weaker winter monsoon signified the smaller contribution of eolian dust, while the stronger summer monsoon represented the larger contribution of terrigenous sediments from the surrounding landmasses and enough sediments weathered from parent rocks for wind to pick up. Meanwhile, the relatively high temperature ensured the high efficiency of weathering rates. However, at 1.3–1.5 Ma BP, the REE contents reversed to be lower levels, despite the SiO_2 contents remained high levels. Notably, both the East Asian summer and winter monsoons were relatively weaker during this interval, which could lead to the low levels of terrigenous constituents. The high levels of SiO_2 at 1.3–1.5 Ma BP may be related to the lagoon deposits related to the sea level fluctuations (Fig. 5). Trace elements, including Si, are highly enriched in the lagoon system, due to the proliferation of algal organisms, as has been observed in a recent study of mesophotic reefs (Abbey et al., 2013). In the Well XK1 of Shidao Island of northern SCS, Shao et al. (2017a) also reported that the detrital elements were enriched in lagoonal facies. In the Well CK2, the reef flat dominated the reef facies prior to ~4.5 Ma BP, except ~1.3–1.5 Ma and ~2.2 Ma BP, when the lagoon facies held the dominant position. Compared to nutrient elements, REE were rarely involved in the vital activities in the open sea. The discrepancy between REE and SiO_2 in chemical property might result in the different situations at 1.3–1.5 Ma BP.

The samples displayed variable $^{87}Sr/^{86}Sr$ isotopic ratios, considerably higher than those expected in open-ocean water masses. We interpreted the highly radiogenic Sr isotopic ratios in some carbonate samples to reflect isotopic exchange with radiogenic Sr from siliciclastic components in the samples according to the geological setting. The radiogenic Sr isotopic ratios might approximate the mixed isotopic composition of seawater in the marginal sea and the eolian dust. The abnormal high values of Sr isotopes beyond the age framework (Fig. 6) appeared mainly during ~1.5–2.6 Ma, indicating the severe impacts from eolian dust. According to Haug and Tiedemann (1998), the Northern Hemisphere ice volume has already increased above its modern level at ~2.7 Ma BP. Actually, the effects of terrigenous dusts on the Sr isotopes of sediments in Xisha Islands (Liu et al., 2014), as well as the western Philippine Sea (Xu et al., 2015), have been confirmed in millennial scale. During this period, the strong winter monsoon and the relatively high temperature as shown in Fig. 5 seemed to be responsible. However, the Sr isotopes tended to be normal after ~1.5 Ma BP, keeping pace with the decrease of REE and SiO_2 contents of the carbonates. It indicated that the effects of terrigenous dusts on Sr isotope were extremely limited. Though East Asian summer and winter monsoons continued to exert influences on the eolian dust and might still dominate the eolian dust after ~1.5 Ma BP through precipitation erosion and transportation, the relative normal intensity of summer and winter monsoon, represented by the loess magnetic susceptibility and the $\delta^{18}O$ of abyssal sediments as shown in Fig. 5, ruled out this possibility. Considering the synchronism of the decreasing of terrigenous constituents and climate cooling, we considered that the continued cooling of the Quaternary contributed to the weakening of continental weathering of the source region of eolian dust transferred to the Xisha Islands.

According to the above discussions, we considered that the continental weathering controlled by the summer monsoon dominated the surface seawater compositions of Xisha Islands before ~2.6 Ma BP, when the winter monsoon was not strong enough to exert significant influences. However, after ~2.6 Ma BP, the effects of aeolian dusts should be considered due to the abrupt intensification of EAWM. The effects of eolian dusts depended on the intensity of EAWM, the precipation driven by summer monsoon, and the temperature. The latter two factors were the major control factors of continental weathering.

7. Conclusions

According to the petrographic, stratigraphical, sedimentological, and elemental and isotope geochemical characteristics from Well CK2, which offered a continuous, highly resolved, well preserved and accurate dated coral reef carbonate record, we provided a systematic coral reef carbonate record from the carbonate platforms in the Yongle atoll of Xisha Islands, northern SCS since Pliocene, with a focus on the environment changes and climate fluctuations. Evidence from the systematic changes of strontium analyses and element compositions of bulk carbonate samples indicated that the elevated terrigenous influences associated with Asian monsoon after the Pliocene. Specifically, the continental weathering controlled by the EASM dominated the surface seawater compositions of Xisha Islands before ~2.6 Ma BP, when the winter monsoon was not strong enough to exert significant influences. However, after ~2.6 Ma BP, the effects of eolian dust should be considered due to the abrupt intensification of EAWM. The effects of

eolian dust depended on the intensity of EAWM, the precipitation driven by summer monsoon, and the temperature, the latter two factors among which were the major control factors of continental weathering. Our results confirmed that the geochemical proxies from bulk carbonates were reliable tools for recording the climate changes, including EAM evolution. However, future research with higher resolution is still required to stress on the records of the shallow-water carbonates.

Acknowledgements

We are grateful to numerous staff members from the Guizhou Bureau of Geology and Mineral Resources, South China Sea Institute of Oceanology and Wuhan Institute of Rock and Soil Mechanics, Chinese Academy of Sciences, for extensive efforts during drilling. This work was financially supported by the National Natural Science Foundation of China (Grant Nos. 91428203, 41603091, and 41663001), the Guangxi scientific projects (Nos. AD17129063, AA17204074 and 2016GXNSFBA380113), and the Bagui Fellowship from Guangxi Province of China (2014BGXZGX03). Thanks are due to the responsible editor and two anonymous reviewers for their critical reviews and constructive comments, which helped us improve our paper significantly.

Data availability

All the new data used in this research have been presented in the main text of the article or as supplementary information.

Appendix A. Supplementary data

Supplementary data to this article can be found online at https://doi.org/10.1016/j.margeo.2019.02.006.

References

Abbey, E., Webster, J.M., Braga, J.C., Jacobsen, G.E., Thorogood, G., Thomas, A.L., Camoin, G., Reimer, P.J., Potts, D.C., 2013. Deglacial mesophotic reef demise on the Great Barrier Reef. Palaeogeogr. Palaeoclimatol. Palaeoecol. 392, 473–494.
Aharon, P., Goldstein, S.L., Wheeler, C.W., Jacobson, G., 1993. Sea-level events in the South Pacific linked with the Messinian salinity crisis. Geology 21, 771–775.
Aïssaoui, D.M., McNeil, D.F., Kirschvink, J.L., 1990. Magnetostratigraphic dating of shallow-water carbonates from Mururoa atoll, French Polynesia: Implications for global eustasy. Earth Planet. Sci. Lett. 97, 102–112.
Alibo, D.S., Nozaki, Y., 2000. Dissolved rare earth elements in the South China Sea: Geochemical characterization of the water masses. J. Geophys. Res. Atmos. 105, 28771–28784.
An, Z., Kutzbach, J.E., Prell, W.L., Porter, S.C., 2001. Evolution of Asian monsoons and phased uplift of the Himalaya-Tibetan plateau since Late Miocene times. Nature 411, 62–66.
Barckhausen, U., Roeser, H.A., 2013. Seafloor Spreading Anomalies in the South China Sea Revisited, Continent-ocean Interactions Within East Asian Marginal Seas. American Geophysical Union, pp. 121–125.
Braithwaite, C.J.R., Dalmasso, H., Gilmour, M.A., Harkness, D.D., Henderson, G.M., Kay, R.L.F., Kroon, D., Montaggioni, L.F., Wilson, P.A., 2004. The Great Barrier Reef: the Chronological Record from a New Borehole. J. Sediment. Res. 74, 298–310.
Cabioch, G., Montaggioni, L., Thouveny, N., Frank, N., Sato, T., Chazottes, V., Dalamasso, H., Payri, C., Pichon, M., Sémah, A.M., 2008. The chronology and structure of the western New Caledonian barrier reef tracts. Palaeogeogr. Palaeoclimatol. Palaeoecol. 268, 91–105.
Cantalejo, B., Pickering, K.T., 2014. Climate forcing of fine-grained deep-marine systems in an active tectonic setting: Middle Eocene, Ainsa Basin, Spanish Pyrenees. Palaeogeogr. Palaeoclimatol. Palaeoecol. 410, 351–371.
Cheng, X., Huang, B., Jian, Z., Zhao, Q., Tian, J., Li, J., 2005. Foraminiferal isotopic evidence for monsoonal activity in the South China Sea: a present-LGM comparison. Mar. Micropaleontol. 54, 125–139.
Clemens, S.C., Murray, D.W., Prell, W.L., 1996. Nonstationary phase of the Plio-Pleistocene Asian Monsoon. Science 274, 943–948.
Derry, L.A., Kaufman, A.J., Jacobsen, S.B., 1992. Sedimentary cycling and environmental change in the Late Proterozoic: evidence from stable and radiogenic isotopes. Geochim. Cosmochim. Acta 56, 1317–1329.
Derry, L.A., Brasier, M.D., Corfield, R.M., Rozanov, A.Y., Zhuravlev, A.Y., 1994. Sr and C isotopes in Lower Cambrian carbonates from the Siberian craton: a paleoenvironmental record during the 'Cambrian explosion'. Earth Planet. Sci. Lett. 128, 671–681.
Du, J., Huang, B., Zhou, L., 2016. Global deepwater circulation between 2.4 and 1.7 Ma and its connection to the onset of Northern Hemisphere Glaciation. Paleoceanography 31, 1480–1497.
Frijia, G., Parente, M., Di Lucia, M., Mutti, M., 2015. Carbon and strontium isotope stratigraphy of the Upper Cretaceous (Cenomanian-Campanian) shallow-water carbonates of southern Italy: Chronostratigraphic calibration of larger foraminifera biostratigraphy. Cretac. Res. 53, 110–139.
Godet, A., Durlet, C., Spangenberg, J.E., Föllmi, K.B., 2016. Estimating the impact of early diagenesis on isotope records in shallow-marine carbonates: a case study from the Urgonian Platform in western Swiss Jura. Palaeogeogr. Palaeoclimatol. Palaeoecol. 454, 125–138.
Guo, Z.T., Ruddiman, W.F., Hao, Q.Z., Wu, H.B., Qiao, Y.S., Zhu, R.X., Peng, S.Z., Wei, J.J., Yuan, B.Y., Liu, T.S., 2002. Onset of Asian desertification by 22 Myr ago inferred from loess deposits in China. Nature 416, 159–163.
Halfar, J., Mutti, M., 2005. Global dominance of coralline red-algal facies: a response to Miocene oceanographic events. Geology 33, 481–484.
Hathorne, E.C., Stichel, T., Brück, B., Frank, M., 2015. Rare earth element distribution in the Atlantic sector of the Southern Ocean: the balance between particle scavenging and vertical supply. Mar. Chem. 177, 157–171.
Haug, G.H., Tiedemann, R., 1998. Effect of the formation of the Isthmus of Panama on Atlantic Ocean thermohaline circulation. Nature 393, 673–676.
He, Q., Zhang, M., 1986. Reef Geology of the Xisha Islands, China. Science Press, Beijing.
Herman, F., Champagnac, J.-D., 2016. Plio-Pleistocene increase of erosion rates in mountain belts in response to climate change. Terra Nova 28, 2–10.
Huang, B., Cheng, X., Jian, Z., Wang, P., 2003a. Response of upper ocean structure to the initiation of the North Hemisphere glaciation in the South China Sea. Palaeogeogr. Palaeoclimatol. Palaeoecol. 196, 305–318.
Huang, B., Jian, Z., Cheng, X., Wang, P., 2003b. Foraminiferal responses to upwelling variations in the South China Sea over the last 220 000 years. Mar. Micropaleontol. 47, 1–15.
Huang, B., Jian, Z., Wang, P., 2005. Paleoceanographic evolution recorded in the northern South China Sea since 4 Ma. Sci. China Ser. D Earth Sci. 48, 2166–2173.
Hutchison, C.S., 2010. The North-West Borneo Trough. Mar. Geol. 271, 32–43.
Jarvis, I., 2001. Geochemistry of pelagic and hemipelagic carbonates: criteria for identifying systems tracts and sea-level change. J. Geol. Soc. Lond. 158, 685–696.
Jia, G., Chen, F., Peng, P.a., 2008. Sea surface temperature differences between the western equatorial Pacific and northern South China Sea since the Pliocene and their paleoclimatic implications. Geophys. Res. Lett. 35, L18609.
Jian, Z., Zhao, Q., Cheng, X., Wang, J., Wang, P., Su, X., 2003. Pliocene–Pleistocene stable isotope and paleoceanographic changes in the northern South China Sea. Palaeogeogr. Palaeoclimatol. Palaeoecol. 193, 425–442.
Jiang, W., Yu, K., Song, Y., Zhao, J.-x., Feng, Y.-x., Wang, Y., Xu, S., Han, T., 2018. Annual REE Signal of East Asian Winter Monsoon in surface seawater in the Northern South China Sea: evidence from a century-long porites coral record. Paleoceanography and Paleoclimatology 33, 168–178.
Kaufman, A.J., Knoll, A.H., 1995. Neoproterozoic variations in the C-isotopic composition of seawater: stratigraphic and biogeochemical implications. Precambrian Res. 73, 27–49.
Kaufman, A.J., Jacobsen, S.B., Knoll, A.H., 1993. The Vendian record of Sr and C isotopic variations in seawater: implications for tectonics and paleoclimate. Earth Planet. Sci. Lett. 120, 409–430.
Kinsey, D.W., Davies, P.J., 1979. Effects of elevated nitrogen and phosphorus on coral reef growth1. Limnol. Oceanogr. 24, 935–940.
Kondo, Y., Takeda, S., Furuya, K., 2007. Distribution and speciation of dissolved iron in the Sulu Sea and its adjacent waters. Deep-Sea Res. II Top. Stud. Oceanogr. 54, 60–80.
Lamy, F., Gersonde, R., Winckler, G., Esper, O., Jaeschke, A., Kuhn, G., Ullermann, J., Martinez-Garcia, A., Lambert, F., Kilian, R., 2014. Increased dust deposition in the Pacific Southern Ocean during glacial periods. Science 343, 403–407.
Li, T., Masuzawa, T., Kitagawa, H., 2004. Seasonal variations in settling fluxes of major components in the oligotrophic Shikoku Basin, the western North Pacific: coincidence of high biogenic flux with Asian dust supply in spring. Mar. Chem. 91, 187–210.
Li, L., Li, Q., Tian, J., Wang, P., Wang, H., Liu, Z., 2011a. A 4-Ma record of thermal evolution in the tropical western Pacific and its implications on climate change. Earth Planet. Sci. Lett. 309, 10–20.
Li, T., Zhao, J., Nan, Q., Sun, R., Yu, X., 2011b. Palaeoproductivity evolution in the centre of the western Pacific warm pool during the last 250 ka. J. Quat. Sci. 26, 478–484.
Liu, T., Ding, Z., Rutter, N., 1999. Comparison of Milankovitch periods between continental loess and deep sea records over the last 2.5 Ma. Quat. Sci. Rev. 18, 1205–1212.
Liu, Y., Sun, L., Zhou, X., Luo, Y., Huang, W., Yang, C., Wang, Y., Huang, T., 2014. A 1400-year terrigenous dust record on a coral island in South China Sea. Sci. Rep. 4, 4994.
Lund, S., Platzman, E., Thouveny, N., Camoin, G., Corsetti, F., Berelson, W., 2010. Biological control of paleomagnetic remanence acquisition in carbonate framework rocks of the Tahiti coral reef. Earth Planet. Sci. Lett. 298, 14–22.
Ma, Y., Wu, S., Lv, F., Dong, D., Sun, Q., Lu, Y., Gu, M., 2011. Seismic characteristics and development of the Xisha carbonate platforms, northern margin of the South China Sea. J. Asian Earth Sci. 40, 770–783.
Martínezgarcía, A., Sigman, D.M., Ren, H., Anderson, R.F., Straub, M., Hodell, D.A., Jaccard, S.L., Eglinton, T.I., Haug, G.H., 2014. Iron fertilization of the Subantarctic ocean during the last ice age. Science 343, 1347–1350.
McArthur, J.M., Howarth, R.J., Bailey, T.R., 2001. Strontium isotope stratigraphy: LOWESS version 3: best fit to the marine Sr-isotope curve for 0–509 Ma and accompanying look-up table for deriving numerical age. J. Geol. 109, 155–170.
McArthur, J.M., Howarth, R.J., Shields, G.A., 2012. Chapter 7 - Strontium Isotope Stratigraphy, the Geologic Time Scale. Elsevier, Boston, pp. 127–144.
McArthur, J.M., Steuber, T., Page, K.N., Landman, N.H., 2016. Sr-isotope stratigraphy:

assigning time in the Campanian, Pliensbachian, Toarcian, and Valanginian. J. Geol. 124, 569–586.
Mclennan, S.M., 2013. Relationships between the trace element composition of sedimentary rocks and upper continental crust. Geochem. Geophys. Geosyst. 2, 2000GC000109.
Ménabréaz, L., Thouveny, N., Camoin, G., Lund, S.P., 2010. Paleomagnetic record of the late Pleistocene reef sequence of Tahiti (French Polynesia): a contribution to the chronology of the deposits. Earth Planet. Sci. Lett. 294, 58–68.
Molnar, P., Boos, W.R., Battisti, D.S., 2010. Orographic Controls on climate and paleoclimate of Asia: thermal and mechanical roles for the Tibetan Plateau. Annu. Rev. Earth Sci. 38, 77–102.
Murray, R.W., Leinen, M., Knowlton, C.W., 2012. Links between iron input and opal deposition in the Pleistocene equatorial Pacific Ocean. Nat. Geosci. 5, 270–274.
Nie, J., Stevens, T., Rittner, M., Stockli, D., Garzanti, E., Limonta, M., Bird, A., Ando, S., Vermeesch, P., Saylor, J., Lu, H., Breecker, D., Hu, X., Liu, S., Resentini, A., Vezzoli, G., Peng, W., Carter, A., Ji, S., Pan, B., 2015. Loess Plateau storage of Northeastern Tibetan Plateau-derived Yellow River sediment. Nat. Commun. 6, 8511.
Nie, J., Pullen, A., Garzione, C.N., Peng, W., Wang, Z., 2018. Pre-Quaternary decoupling between Asian aridification and high dust accumulation rates. Sci. Adv. 4, eaao6977.
Ogg, J.G., 2012. Geomagnetic Polarity Time Scale. Geologic Time Scale, pp. 85–113.
Pagani, M., Zachos, J.C., Freeman, K.H., Tipple, B., Bohaty, S., 2005. Marked decline in atmospheric carbon dioxide concentrations during the Paleogene. Science 309, 600–603.
de Paula-Santos, G.M., Caetano-Filho, S., Babinski, M., Enzweiler, J., 2018. Rare earth elements of carbonate rocks from the Bambuí Group, southern São Francisco Basin, Brazil, and their significance as paleoenvironmental proxies. Precambrian Res. 305, 327–340.
Rea, D.K., Snoeckx, H., Joseph, L.H., 1998. Late Cenozoic Eolian deposition in the North Pacific: Asian drying, Tibetan uplift, and cooling of the northern hemisphere. Paleoceanography 13, 215–224.
Robinson, S.A., 2011. Shallow-water carbonate record of the Paleocene-Eocene Thermal Maximum from a Pacific Ocean guyot. Geology 39, 51–54.
Rohling, E.J., Foster, G.L., Grant, K.M., Marino, G., Roberts, A.P., Tamisiea, M.E., Williams, F., 2014. Sea-level and deep-sea-temperature variability over the past 5.3 million years. Nature 508, 477–482.
Saltzman, M.R., 2005. Phosphorus, nitrogen, and the redox evolution of the Paleozoic oceans. Geology 33, 573–576.
Self-Trail, J.M., Robinson, M.M., Bralower, T.J., Sessa, J.A., Hajek, E.A., Kump, L.R., Trampush, S.M., Willard, D.A., Edwards, L.E., Powars, D.S., Wandless, G.A., 2017. Shallow marine response to global climate change during the Paleocene-Eocene Thermal Maximum, Salisbury Embayment, USA. Paleoceanography 32, 710–728.
Shackleton, N.J., 1995. Pliocene stable isotope stratigraphy of site 846. Proc. ODP Sci. Results 138, 337–355.
Shackleton, N.J., Opdyke, N.D., 1977. Oxygen isotope and palaeomagnetic evidence for early Northern Hemisphere glaciation. Nature 270, 216.
Shackleton, N.J., Backman, J., Zimmerman, H., Kent, D.V., Hall, M.A., Roberts, D.G., Schnitker, D., Baldauf, J.G., Desprairies, A., Homrighausen, R., 1984. Oxygen isotope calibration of the onset of ice-rafting and history of glaciation in the North Atlantic. Nature 307, 620–623.
Shao, Y., Wyrwoll, K.H., Chappell, A., Huang, J., Lin, Z., Mctainsh, G.H., Mikami, M., Tanaka, T.Y., Wang, X., Yoon, S., 2011. Dust cycle: an emerging core theme in Earth system science. Aeolian Res. 2, 181–204.
Shao, L., Cui, Y., Qiao, P., Zhang, D., Liu, X., Zhang, C., 2017a. Sea-level changes and carbonate platform evolution of the Xisha Islands (South China Sea) since the Early Miocene. Palaeogeogr. Palaeoclimatol. Palaeoecol. 485, 504–516.
Shao, L., Li, Q., Zhu, W., Zhang, D., Qiao, P., Liu, X., You, L., Cui, Y., Dong, X., 2017b. Neogene carbonate platform development in the NW South China Sea: Litho-, bio- and chemo-stratigraphic evidence. Mar. Geol. 385, 233–243.
Siahi, M., Hofmann, A., Master, S., Wilson, A., Mayr, C., 2018. Trace element and stable (C, O) and radiogenic (Sr) isotope geochemistry of stromatolitic carbonate rocks of the Mesoarchaean Pongola Supergroup: Implications for seawater composition. Chem. Geol. 476, 389–406.
Song, Y., Fang, X., Li, J., An, Z., Miao, X., 2001. The late Cenozoic uplift of the Liupan Shan, China. Sci. China Earth Sci. 44, 176–184.
Sun, D., Liu, D., Chen, M., An, Z., John, S., 1997. Magnetostratigraphy and palaeoclimate of Red Clay sequences from Chinese Loess Plateau. Sci. China Earth Sci. 40, 337–343.
Sun, D., An, Z., Shaw, J., Bloemendal, J., Sun, Y., 1998. Magnetostratigraphy and palaeoclimatic significance of Late Tertiary aeolian sequences in the Chinese Loess Plateau. Geophys. J. Int. 134, 207–212.
Tauxe, L., Butler, R.F., Van, d.V., R., Banerjee, S.K., 2010. Essentials of Paleomagnetism. University of California Press.
Taylor, S.R., McLennan, S.M., 1985. The Continental Crust: Its Composition and Evolution. Blackwell, Oxford.
Wan, S., Li, A., Clift, P.D., Stuut, J.-B.W., 2007. Development of the East Asian monsoon: Mineralogical and sedimentologic records in the northern South China Sea since 20 Ma. Paleogeogr. Paleoclimatol. Paleoecol. 254, 561–582.
Wan, S., Clift, P.D., Li, A., Yu, Z., Li, T., Hu, D., 2012. Tectonic and climatic controls on long-term silicate weathering in Asia since 5 Ma. Geophys. Res. Lett. 39, 151–155.
Wang, L., Sarnthein, M., Erlenkeuser, H., Grimalt, J., Grootes, P., Heilig, S., Ivanova, E., Kienast, M., Pelejero, C., Pflaumann, U., 1999a. East Asian monsoon climate during the Late Pleistocene: high-resolution sediment records from the South China Sea. Mar.Geol. 156, 245–284.
Wang, L., Sarnthein, M., Grootes, P.M., Erlenkeuser, H., 1999b. Millennial reoccurrence of century-scale abrupt events of East Asian Monsoon: a possible heat conveyor for the global deglaciation. Paleoceanography 14, 725–731.
Wang, P., Zhao, Q., Jian, Z., Cheng, X., Huang, W., Tian, J., Wang, J., Li, Q., Li, B., Su, X., 2003. Thirty million year deep-sea records in the South China Sea. Chin. Sci. Bull. 48, 2524–2535.
Webb, G.E., Kamber, B.S., 2000. Rare earth elements in Holocene reefal microbialites: a new shallow seawater proxy. Geochim. Cosmochim. Acta 64, 1557–1565.
Wei, G., Liu, Y., Li, X., Chen, M., Wei, W., 2003. High-resolution elemental records from the South China Sea and their paleoproductivity implications. Paleoceanography 18, 1054.
Wei, G., Li, X.-H., Liu, Y., Shao, L., Liang, X., 2006. Geochemical record of chemical weathering and monsoon climate change since the early Miocene in the South China Sea. Paleoceanography 21, PA4214.
Wilson, M.E.J., 2008. Global and regional influences on equatorial shallow-marine carbonates during the Cenozoic. Palaeogeogr. Palaeoclimatol. Palaeoecol. 265, 262–274.
Wu, S., Yang, Z., Wang, D., Lü, F., Lüdmann, T., Fulthorpe, C., Wang, B., 2014. Architecture, development and geological control of the Xisha carbonate platforms, northwestern South China Sea. Mar. Geol. 350, 71–83.
Wu, C.-C., Shen, C.-C., Lo, L., Hsin, Y.-C., Yu, K., Chang, C.-C., Lam, D.D., Chou, Y.-M., Liu, Y., Pallister, J., Song, S.-R., Chiang, H.-W., Burr, G.S., 2018. Pinatubo volcanic eruption exacerbated an abrupt coral mortality event in 1991 summer. Geophys. Res. Lett. 45, 2018GL079529.
Xiong, Z., Li, T., Crosta, X., Algeo, T., Chang, F., Zhai, B., 2013. Potential role of giant marine diatoms in sequestration of atmospheric CO_2 during the Last Glacial Maximum: $\delta^{13}C$ evidence from laminated Ethmodiscus rex mats in tropical West Pacific. Glob. Planet. Chang. 108, 1–14.
Xu, Z., Li, T., Wan, S., Yin, X., Jiang, F., Sun, H., Choi, J., Lim, D., 2014. Geochemistry of rare earth elements in the mid-late Quaternary sediments of the western Philippine Sea and their paleoenvironmental significance. Sci. China Earth Sci. 57, 802–812.
Xu, Z., Li, T., Clift, P.D., Lim, D., Wan, S., Chen, H., Tang, Z., Jiang, F., Xiong, Z., 2015. Quantitative estimates of Asian dust input to the western Philippine Sea in the mid-late Quaternary and its potential significance for paleoenvironment. Geochem. Geophys. Geosyst. 16, 3182–3196.
Yu, K., 2012. Coral reefs in the South China Sea: their response to and records on past environmental changes. Sci. China Earth Sci. 55, 1217–1229.
Yu, K., Zhao, J., 2009. Coral reefs. In: Wang, P., Li, Q. (Eds.), The South China Sea: Paleoceanography and Sedimentology. Springer Netherlands, Dordrecht, pp. 229–254.
Zachos, J., Pagani, M., Sloan, L., Thomas, E., Billups, K., 2001. Trends, rhythms, and aberrations in global climate 65 Ma to present. Science 292, 686–693.
Zhang, J., Wang, P., Li, Q., Cheng, X., Jin, H., Zhang, S., 2007. Western equatorial Pacific productivity and carbonate dissolution over the last 550 kyr: foraminiferal and nannofossil evidence from ODP Hole 807A. Mar. Micropaleontol. 64, 121–140.
Zheng, H., Mcaulay Powell, C., An, Z., Zhou, J., Dong, G., 2000. Pliocene uplift of the northern Tibetan Plateau. Geology 28, 715–718.